# Crash Area Estimation for Ground Risk of Small Unmanned Aerial Vehicles Due to Propulsion System Failures

Mohd Hasrizam Che Man[1]
*Air Traffic Management Research Institute (ATMRI), Nanyang Technological University*
*65 Nanyang Drive, 637460, Singapore*

Haoliang Hu[2] and Kin Huat Low[3]
*School of Mechanical and Aerospace Engineering, Nanyang Technological University*
*50 Nanyang Avenue, 639798, Singapore*

**Drones or Unmanned Aerial Vehicles (UAVs) are expected to be used for different applications like parcel delivery, inspection, and aerial photography in the urban area. However, UAVs usually uses an electric system to power up the propulsion, communications, navigation, and flight control system, which means it is not as reliable as the manned aircraft system and may result in failure during operation and then crash to the ground. At present, there is almost no publication about the high-fidelity modeling used by UAVs to calculate the crash trajectory and point of crash. The experimental data for modeling and simulation verification of multi-rotor aircraft is limited. So far, crash trajectory prediction has been limited to point mass or ballistic methods, and these methods are usually only suitable for complete power failure and without any control system. This study intends to investigate the effects of different UAV failure modes on its crash trajectory and crash area compared to the ballistic model by using ADAMS and MATLAB co-simulation methods. Conclusions from the study show the crash trajectory, flight distance and impact speed of the UAV under four failure modes, which are quite different from the ballistic trajectory. The findings can potentially contribute to better risk assessment of the multi-rotor sUAV in the urban environment operation.**

## I. Nomenclature

| | | |
|---|---|---|
| $\phi$ | = | roll angle |
| $\theta$ | = | pitch angle |
| $\psi$ | = | yaw angle |
| $\rho$ | = | air density |
| $\Omega$ | = | difference between the sum of angular velocities of motor 2, 4 and the sum of angular velocities of motor 1, 3 |
| $C_D$ | = | coefficient of drag |
| $D$ | = | drag force |
| $F$ | = | force generated by a propeller |
| $H$ | = | sum of absolute moments of momentum |
| $I_x$ | = | moment of inertia (x-axis) |
| $I_y$ | = | moment of inertia (y-axis) |

[1] Research Associate, Air Traffic Management Research Institute, Nanyang Technological University (NTU)
[2] Post-graduate Research Student, School of Mechanical and Aerospace Engineering, NTU.
[3] Professor, School of Mechanical and Aerospace Engineering, NTU; Corresponding Author: mkhlow@ntu.edu.sg

$I_z$ = moment of inertia (z-axis)
$J_{RP}$ = total moment of inertia of the motor rotor and propeller rotating around the motor shaft
$M$ = sum of external moments of the drone
$m$ = mass of the drone
$p$ = roll rate
$q$ = pitch rate
$r$ = yaw rate
$S$ = windward area of the drone in frontal (side) and planform views
$S_{rf}$ = real frontal area of the drone
$S_{rt}$ = real planform area of the drone
$S_f$ = frontal area of the drone
$S_t$ = planform area of the drone
$U_1$ = vertical speed control quantity
$U_2$ = roll speed control quantity
$U_3$ = pitch speed control quantity
$U_4$ = yaw speed control quantity
$V$ = velocity of the drone relative to air
$v$ = centroid velocity of the drone
$x$ = displacement (x-direction)
$y$ = displacement (y-direction)
$z$ = displacement (z-direction)

## II. Introduction

The use of unmanned aerial vehicles (UAVs) has attracted a lot of attention due to its potential for different applications, such as parcel delivery, industrial inspection, and urban air mobility [1]. However, the risk associated with the drone operation in such an environment is still not fully understood, especially for operation within an urban environment and near aerodrome airspace. Currently, regulatory bodies like FAA [2] have restricted a UAV, whose weight is less than 25 kg, should be operated 5 km from aerodrome airspace [3], under Visual Line-of-Sight (VLOS) and not above the crowd.

In order to enable full drone operation in urban or near aerodrome airspace, the associated risk to its operation has to be investigated carefully. A few studies have investigated the risks of a drone operation to the people and vehicles on the ground in urban low altitude airspace [4-7] and damage severity due to drone intrusion into aerodrome airspace [8-10]. In addition, some studies have developed a drone risk-based model assessment for path-planning by considering different third-party risks scenario [11, 12].

Reliability and fault of the drone is one factor that requires special attention to identifying risk in urban and near aerodrome airspace, a study by [13] reported small unmanned aerial vehicles (sUAV) has low reliability compared to commercial aircraft by taking the reliability of sUAV electronic similar as common electronics devices (such as computer disk drives). To understand this situation, some study has simulated a lot of failures scenarios and observed the dynamics of unpowered aircraft to determine the affected area and possible range of these failures [14, 15]. The study concluded that most crashes occurred near the initial failure location. Similarly, [16] expresses the potential crash area as an equation between the aircraft's weight, speed, direction, and maximum taxi distance.

The recent research by [17] provided the simulation and prediction of the trajectory of the multi-rotor during propulsion failure and provided the prediction of the roll mode and the resulting near-ballistic trajectory in the event of a sudden motor failure. NASA [18] has researched real-time trajectory prediction of UAS aircraft. The predicted descent rate and wind speed have proposed an impact point prediction algorithm to estimate the trajectory from termination to ground impact. [14] used differential equation of the standard second-order drag model suitable for the aircraft debris scene, proposing the probability density function of the UAV's ground crash area. Most of the models proposed from the previous research [15-17, 19] use a relatively simple method to predict the trajectory and impact point. The high-precision prediction of the impact point plays a vital role in the risk assessment of the casualty estimation module [20].

The descent model assumed all the drone parts faulted at the same time. However, a certain type of failure might lead to severe damage and higher risks as some drone parts might have better reliability and occur at different times. Studies by [21, 22] show, drone system failure can be divided into five categories: power /propulsion failure, flight control system failure, human/ground error, communications failure and miscellaneous. This research showed that more than 63% of accidents resulting in significant damage or total loss are caused by power/propulsion failure and

flight control system failure. Hence, the assumption used for the current descent model might not be sufficient to represent the realistic scenario for the drone risk assessment model.

So far, trajectory prediction has been limited to point mass or ballistic methods, and these methods are usually only suitable for complete power failure and without any control system. Therefore, the objective of this paper is to extend the current model for evaluation of the crash trajectory and speed of a quad-rotor drone by considering different scenarios, like partial power loss, flight control system failure or a combination of different drone failures.

This study aims to evaluate the trajectory speed and crash area caused by different drone propulsion system failures. This paper analyzes the impact performance of the quad-rotor UAV at the height of 60 m (the highest altitude allowed without approval for small drones in Singapore [23]), a high-fidelity drone model is proposed, and the most common drone failure types are analyzed. According to the corresponding failure form, MATLAB has used the form of co-simulation with ADAMS to obtain results, including crash time, crash speed, crash trajectory, and impact point. The research in this paper is expected to make a certain contribution to the risk assessment of future multi-rotor sUAV and the corresponding path planning [14, 18] by proposing a method to evaluate the crash trajectory and path of the drone, the inherent risk of impact can be controlled and reduced through mitigation measures.

## III. Dynamic Analysis of Quadrotor UAV

### A. Validation of Windshield Material Model

The mechanical model in the coordinate system of the four-rotor UAV can be shown in Fig. 1. The four evenly distributed rotors produce corresponding thrust and torque according to the corresponding speed [24]. In addition, the drone body will also be subject to uniformly distributed gravity and air resistance that needs to be calculated.

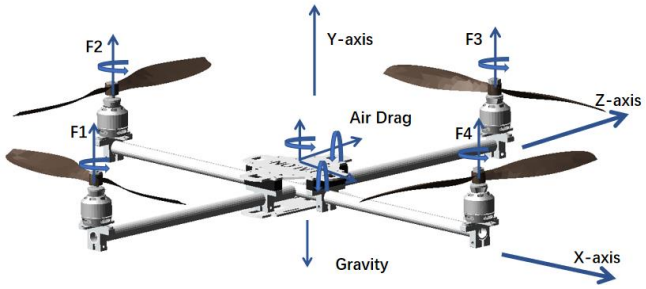


Fig. 1 Forces that acting on the Talon quad-rotor UAV model which considered in this study.

Quad-rotor UAV is a non-coaxial multi-rotor aircraft that can take off and land vertically. One group of motors on the same diagonal rotates counterclockwise, and the other group rotates clockwise, which cancels out the rotation band of the motors. By adjusting the rotational speed of the four symmetrically distributed motors, the anti-torque force can continuously change the position of the UAV and realize the control of the flight attitude, such as hovering, pitching, lifting, and rolling.

The drone has 4 inputs (4 channels) and 6 degrees of freedom output. According to different motor layouts, sUAV can be divided into "+" and "×" types. This article mainly focused on the "+" layout. According to Newton's second law, the flight dynamics equation can be expressed as:

$$F = m\frac{v}{dt}$$
$$M = m\frac{H}{dt} \quad (1)$$

According to the control method of the UAV [25], the nonlinear coupling model is decomposed into 4 independent control channels:

$$U_1 = F_1 + F_2 + F_3 + F_4$$
$$U_2 = F_4 - F_2$$
$$U_3 = F_3 - F_1$$
$$U_4 = F_2 + F_4 - F_3 - F_1 \quad (2)$$

Without considering the resistance, the resultant mathematical model is obtained as follows:

$$\begin{aligned}
\ddot{x} &= \frac{U_1}{m}(cos\,\psi\,sin\,\theta\,cos\,\phi + sin\,\psi\,sin\,\phi) \\
\ddot{y} &= \frac{U_1}{m}cos\,\psi\,cos\,\theta - g \\
\ddot{z} &= \frac{U_1}{m}(sin\,\psi\,sin\,\theta\,cos\,\phi + cos\,\psi\,sin\,\phi) \\
\ddot{\phi} &= \frac{1}{I_x}[U_3 + qr(I_z - I_y) - J_{RP}\Omega) \\
\ddot{\theta} &= \frac{1}{I_z}[U_2 + qr(I_y - I_z) + J_{RP}\Omega)] \\
\ddot{\psi} &= \frac{1}{I_y}[U_4 + pq(I_x - I_z)]
\end{aligned} \tag{3}$$

**B. Maintaining the Integrity of the Specifications**

It is foreseeable that when single or multiple motors fail or blades fall off, the asymmetric lift and the corresponding moments generated on the remaining motors will cause the drone body to rotate in the direction of the failed motors, as shown in Fig. 2, within 0.10 s to 0.30 s after the sudden failure of one/multiple motors of the drone, the drone started to rotate in different directions. When the control system can still work, it will continue to control the remaining rotors and try to adjust the drone back to the state before the failure occurs (actually, in most cases, a controllable flight can no longer be achieved). It also affects the thrust and torque of the drone during the crash to a certain extent and changes the impact trajectory.

*t* = 0.10 s *t* = 0.15 s *t* = 0.20 s *t* = 0.25 s *t* = 0.30 s

Fig. 2 Schematic diagram of drone body rotations in the direction of failed motor.

According to the common failure modes of quad-rotor UAVs analyzed in the first chapter, select the conditions that will significantly impact the trajectory of the UAV. There are four possible propulsion system failures:

1. Single motor of the drone completely stops working due to the electrical fault or mechanical fault, and the drone's flight control system the remaining three drone motors continue to be working in perfect condition.
2. The drone's single motor and flight control system is not working simultaneously, and the remaining three drone motors continue to rotate at a fixed rotation speed before crashing.
3. Two motors of the drone stopped working due to an electrical fault or mechanical fault, and the drone's flight control system the remaining two drone motors continue to be working in perfect condition.
4. Propeller of a single motor is loose and fall off during flight.

## IV. Methodology of Analysis

**A. Co-simulation by using Different Software**

ADAMS is widely used for virtual prototype simulation and optimization. ADAMS is one of the most widely used dynamic simulation software in the field of mechanical design [26]. It is mainly composed of interface ADAMS/view, solver ADAMS/Solver and ADAMS/Post Processor. Test simulation and analysis of a kind of virtual prototype. MATLAB has powerful matrix calculation capabilities as a commercial mathematics software, and it is widely used to perform drone flight simulations or control simulations [16]. There have been a lot of cases of joint simulation between these two.

The Simulink module in MATLAB is usually used for co-simulation with ADAMS. First, the corresponding model needs to be established in ADAMS. In view of the slightly insufficient modeling capabilities of Adams, the corresponding multi-rotor UAV can be established in other software, such as Solidworks. After a certain degree of simplification, the model is imported into ADAMS in the Parasolid format (.x_t). After adding the relevant dynamic parameters, the mechanical system export in ADAMS Controls plug-in of ADAMS exports the model in the form of a bin file, and all input and output will enter and exit the model in the form of dynamic variables. ADAMS_sub is the model imported by ADAMS into the MATLAB Simulink. The input and output data can form a closed-loop control. The logic diagram of the co-simulation model is shown in Fig. 3. Solidworks is used to construct the model, ADAMS conducts dynamic simulation, and MATLAB is responsible for the calculated model.

**B. MATLAB Simulink Model Setup**

In the co-simulation, the MATLAB Simulink module is the core component responsible for calculating the dynamic output required by the UAV model in ADAMS and accepting the kinematic output generated by the UAV model in ADAMS. As shown in Fig.4, it is mainly composed of the ADAMS UAV model module, control module, air resistance (aerodynamic) calculation module, wind calculation module, and the rotor lift and torque conversion module.

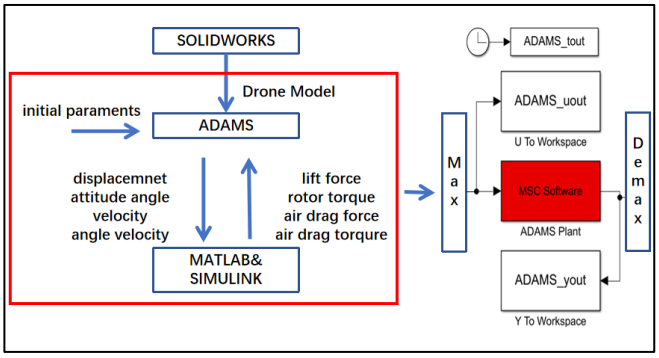


Fig. 3 The logic diagram of input and output between Solidworks, ADAMS and MATLAB Simulink.

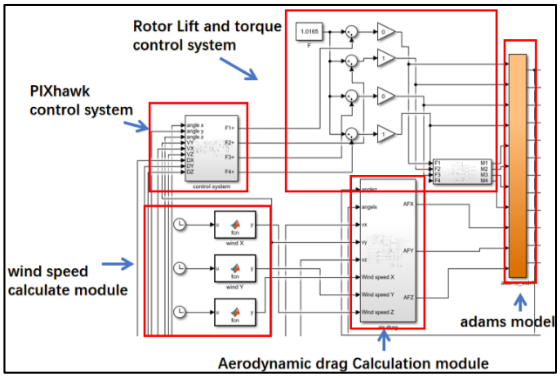


Fig. 4 Co-simulation model interface using MATLAB Simulink.

In the aerodynamic drag calculation module, the influences of the changing windward area of the different views and the changing velocities during the crash are considered by

$$D = \frac{1}{2} C_D \rho V^2 S \qquad (4)$$

The velocities of the drone can be obtained directly from the simulation as outputs. Since the quad-rotor UAV has a symmetric structure for the windward area, its side view area is the same as the front view area. Therefore, we have

$$\begin{aligned} S_{rf} &= S_f \cdot cos(\theta)\, cos(\phi) + S_t \cdot sin(\theta)\, sin(\phi) \\ S_{rt} &= S_t \cdot cos(\theta)\, cos(\phi) + S_f \cdot sin(\theta)\, sin(\phi) \end{aligned} \qquad (5)$$

The wind speed model is modified in real-time according to the local wind map, and it should be function about the height. The control system can be chosen from the existing control system module in the MATLAB database, such as PX4, the Pixhawk 1 flight control systems. The motor lifts and torque control system are used to simulate the failure situation of the UAV by controlling the gain to 0 of each module. Other modules in the figure are scopes used to view the different result curves of the simulation.

## V. Model Parameter Setup

**A. Drone Model Setup**

The present study is based on a small Talon quad-rotor drone as a demonstration. The UAV model parameters used are simplified to a certain extent while maintaining the actual characteristics. The parameters of the simplified UAV and its rotor are shown in Table 1.

In the present study, air resistance is considered, and the drag torque generated by air is not considered. In Eq. (4), the $C_D$ is defined as 0.4, $\rho$ as of 1.225 kg/m$^3$, $V$ and $S$ in the three coordinate axis directions supplied by the simulation

module. In the aerodynamic calculation module shown in Figs. 5(b) and 5(c), the windward area of the planform view and the frontal view (considering the pendent) of the quad-rotor drone are estimated. Among them, the frontal area is estimated to be 0.01698m$^2$, and the planform area is estimated as 0.02167m$^2$.

To use the high-fidelity model, first, use Solidworks to build the model of the Quadrotor UAV. The model has simplified the motor, motor arm, motor bracket, main top plate and main bottom plate of the drone are retained. The initial material is steel by default, and then the assembly file is imported into ADAMS for definition and modification in the format of Parasolid (.x_t). The UAV mainly includes the definition of materials and the addition of fixed pairs. Simplification of the drone model done by deleting the redundant adjacent parts by modifying the density, combined with the materials that come with ADAMS, the material definition and the parts naming of the drone is shown in Table 2 and Fig. 6.

Table 1 UAV Model parameters.

| UAV attributes | Parameter |
|---|---|
| Long rotor arm length | 48.8 cm |
| Long rotor arm length | 22. 4cm |
| Total mass | 0.476 kg |
| Single rotor mass | 57 g |
| Rotor lift: range | 0-20 N |
| Rotor lift: torque | 1N:0.8 N/M |

Table 2 Material definition of the drone.

| Part | Material |
|---|---|
| Riser Mount | Carbon fiber epoxy |
| Talon Top Plate | Steel |
| Motor Mount | Carbon fiber prepreg |
| Motor | Aluminum |
| Arm | Carbon fiber prepreg |
| Talon bottom Plate | Steel |

The model's input is defined as the four motor lifting forces, moments, and air resistance in three directions, totaling 11 forces and moments labelled as F1-F4, M1-M4, AF1-AF3. Considering the force acting on the drone, additional forces and moments are added to the drone model, including gravity, the lift generated by the 4 motors and its corresponding moments, and define the air resistance along with the Cartesian coordinate system as AF1, AF2, AF3 which then defined as the state variables in ADAMS for the UAV input and output.

The output is defined as the displacement UAV ‘s center of mass displacement, angular displacement, velocity, and angular velocity along the three coordinate axes, a total of 12 outputs, as shown in Fig.1, the naming order of F1-F4 is marked, as well as the three-axis Cartesian coordinate system defined direction. After the definition was completed, the model was exported to MATLAB for co-simulation through the control system's output in ADAMS.

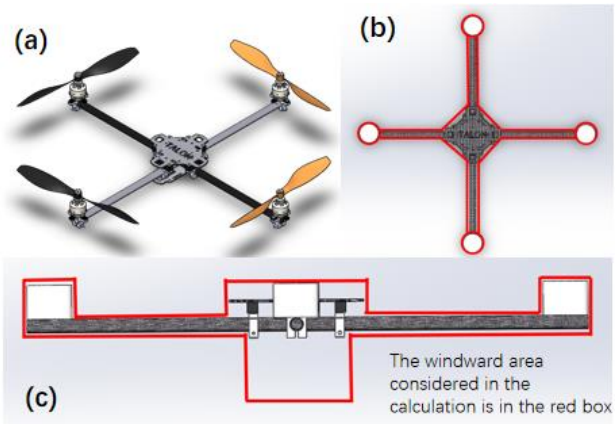


Fig. 5 The estimation area of the drone: (a) isometric view (b) the top view and (c) the front view of the UAV model. The windward area considered in the calculation is in the red box.

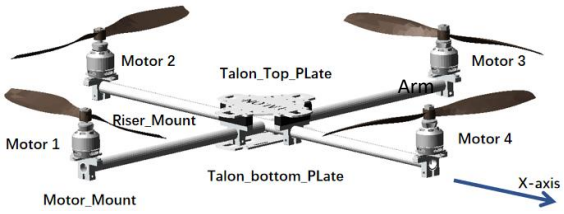


Fig. 6 Name definition for the drone parts.

**B. Control System Parameters Setup**

This article is Among them, the control module adopts the most common flight control system PIXHAWK 1 control method in the UAV control module and imports the PX4 module in the MATLAB 2020 resource library and modifies it so that it can be paired with the model in ADAMS, as shown in Fig. 7. In this model, the position and

altitude controller have been modified to velocity and altitude controller, which means this controller will control the drone fly at a constant speed. The relative PID parameters are shown in Table 3; the output of this flight control system model will directly in the form of thrust force in 4 motors instead of RPM, and then come into torques calculate model to become torque and be sent to ADAMS together with the thrust forces.

The wind resistance is calculated during the drone's flying using the air resistance calculation formula presented in Eq. (4). The wind speed model can be modified in real-time according to the local wind map, and to simplify the analysis in this paper, it is assumed that the wind speed in all directions is 0 to simulate a no wind condition. After completing this step, the simulation model is built.

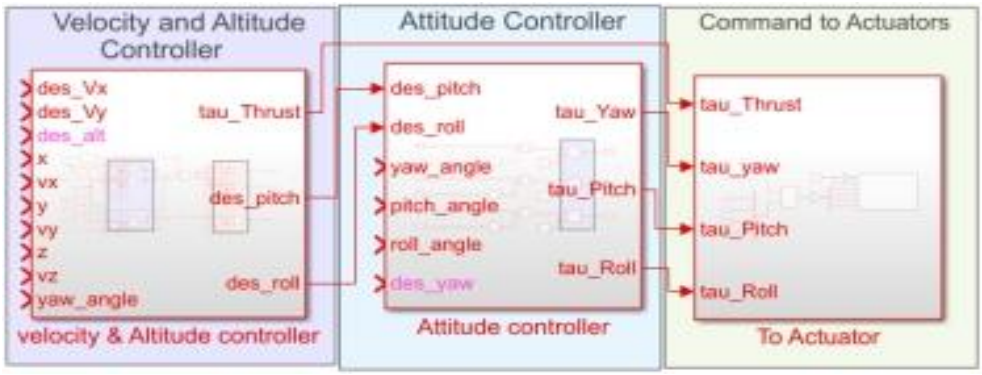


Fig. 6 Model of Flight control system (FCS) for PIXHAWK 1.

According to the previously analyzed failure situations, the conditions of the four motors are controlled by adjusting the lift and torque control modules to simulate various failure situations. In this study, flight control system failures, blade Loose or fall off are mainly considered. Various failure forms and their corresponding motor conditions are shown in Table 4.

Table 3 PID Parameters.

| CONTROLLER | PID PARAMETERS | GAIN |
|---|---|---|
| PITCH ANGLE FOR VELOCITY X | (5 10 2) | 0.001 |
| ROLL ANGLE FOR VELOCITY Y | (5 20 5) | 0.001 |
| ROLL ANGLE | (5 20 5) | 1 |
| YAW ANGLE | (5 20 5) | 1 |
| PITCH ANGLE | (5,20 1) | 1 |
| THRUST | (5 10 2) | 1 |

Table 4 Motor conditions in different fault types.

| Fault Types | Lift and Torque Setting |
|---|---|
| Flight control system (FCS) | Set Control module parameter to 0 in the Simulink module. |
| Blade Loose or Fall-off | Set 1-3 of F1-F4 to 0 when keeping their torque. |
| Power Failures | Decrease all motors lift and torques to 0. |
| Motor Failures | Decrease single or multiple motors lift and torques to 0. |

## VI. Results and Discussions

In this section, the UAV crash area and trajectory from the simulation works will be presented and discussed. Two cases are considered in the simulation; the first is failure that might lead to total thrust loss, the second is UAV fault that might lead to partial thrust loss and some other faults. In the second case, the position and number of failed motors or propellers and whether the control system is involved in flight control can be divided into the following five

situations. Each situation is compared with the simulation results of the first case (the situation when the power totally failed.

The initial height of 60 m is defined, the impact positions and the corresponding impact speeds are shown in Table 5. Note that R1-R4 in Table 5 represents motor1-motor4 (R means the motor's rotor), and the array in parentheses represents the coordinates of the impact site after the drone crash at the height of 60 m. In the Cartesian right-hand coordinate system, take the flying direction of the drone as the positive *x*-axis and the vertical direction as the *z*-axis. Set the initial position of the drone as (0, 0, 60), and then the impact point coordinates should be (*x*, *y*, 0). The data outside the brackets represents the velocity when the drone impacts the ground surface from a height of 60 m.

Table 5 Impact positions on the ground and the corresponding impact velocity at an initial height of 60 m.

| **Failure Modes** | **Faulty Parts** | **Forward Speed** | | | |
|---|---|---|---|---|---|
| | | **0 m/s** | | **8 m/s** | |
| | | **Displacement (m)** | **Impact Velocity (m/s)** | **Displacement (m)** | **Impact Velocity (m/s)** |
| One motor (with control system) | R1 | (-3.28, -0.08) | 25.17 | (23.16, 0.81) | 31.40 |
| | R2 | (-0.67, 9.7) | 20.08 | (32.52,15.01) | 21.82 |
| | R3 | (3.52, 0.21) | 24.30 | (33.25, 3.38) | 23.25 |
| | R4 | (0.62, -9.42) | 19.10 | (31.63, -8.51) | 27.02 |
| One motor (without control system) | R1 | (47.20, 6.50) | 18.70 | (1.35, 5.09) | 15.93 |
| | R2 | (1.71, 65.81) | 26.40 | (48.83, 66.14) | 27.08 |
| | R3 | (36.43, 1.44 ) | 42.13 | (84.54, 1.29) | 19.51 |
| | R4 | (6.81, 64.10) | 26.26 | (53.04, -63.45) | 26.83 |
| One blade fell-off (with control system) | BLADE 1 | (-4.97, 1.86) | 45.01 | (52.04, 25.62) | 22.89 |
| | BLADE 2 | (-19.68, 17.26) | 50.02 | (23.02, 20.38) | 47.01 |
| | BLADE 3 | (8.80, -14.60) | 22.15 | (60.13, -21.50) | 49.71 |
| | BLADE 4 | (16.03, -16.99) | 29.68 | (29.14, -8.51) | 31.40 |
| Two motors (with flight control system | R1 R2 | (1.30, -1.04) | 25.14 | (54.05, 12.90) | 31.84 |
| | R1 R3 | (-6.36, -0.14) | 31.46 | (14.55, 15.82) | 29.22 |
| | R1 R4 | (-0.96, 0.74) | 46.60 | (25.19, 1.05) | 34.66 |
| | R2 R3 | (3.01, -2.36) | 30.39 | (21.02, 0.68) | 52.50 |
| | R2 R4 | (0.82, -0.02) | 25.24 | (30.01, -0.02) | 26.20 |
| | R3 R4 | (-0.59, -0.62) | 24.60 | (39.99, 2.77) | 18.99 |
| Power | R1 R2 R3 R4* | (0.00, 0.00) | 24.61 | (27.42, 0.0) | 25.66 |

*By assuming all four motors are faulty due to power failure (baseline configuration).

**A. One (1) motor failed with/without flight control system (hovering; zero initial forward velocity)**

When the initial forward velocity is 0 m/s (hovering), one motor fails, and the control system can still work, the simulation results of the drone's trajectory, the projection of the trajectory on the ground and the curve of the drone's velocity and altitude with time are shown in Fig. 8(a), Fig. 8(c), and Fig. 9, respectively. The possible collision area is small, distributed in a circle with a radius of less than 20 m, and collides with the ground faster than in the case of power failure.

When one motor fails, and the flight control system is not working, the projection of the trajectory on the ground and the curve of drone velocity and height time histories are shown in Fig. 8(b), Fig. 8(d), and Fig.10, respectively. The possible crash area is large, distributed in a circle with a radius of around 50 m.

The impact time is longer than in the case of power failure. In terms of impact velocity, the rotation of the drone body caused by the unbalanced torque makes the drone move in all directions, and acceleration occurs. Although the initial acceleration is less than a free fall, the final impact velocity under the influence of air drag force is nearly the same as that of the case of power failure.

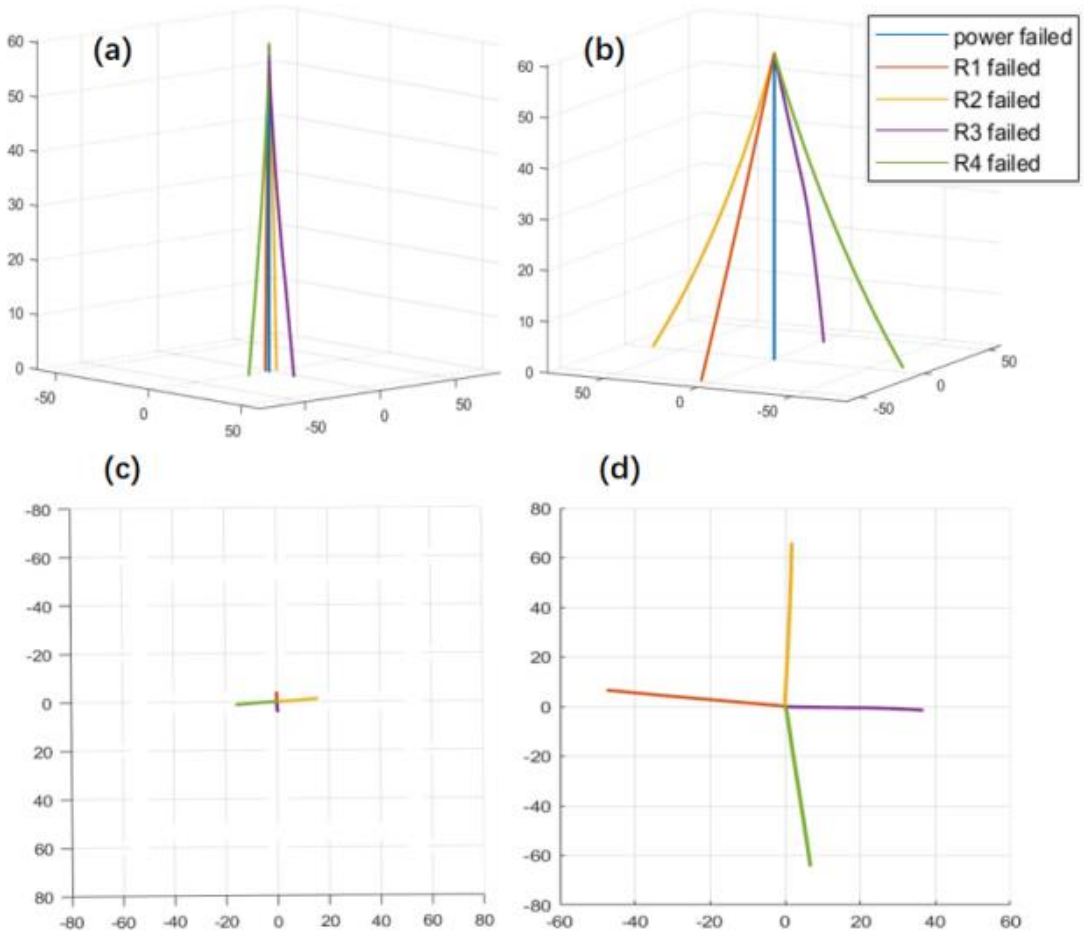


Fig. 7 Results for initial forward velocity is 0 m/s (hovering) with one motor failed and with/without flight control system: (a) the trajectories when initial velocity is 0m/s when control system is working; (b) the trajectories when initial velocity is 0m/s when flight control system failed.; (c) the projection of the trajectory on the ground when control system is working; and (d) the projection of the trajectory on the ground when flight control system failed.

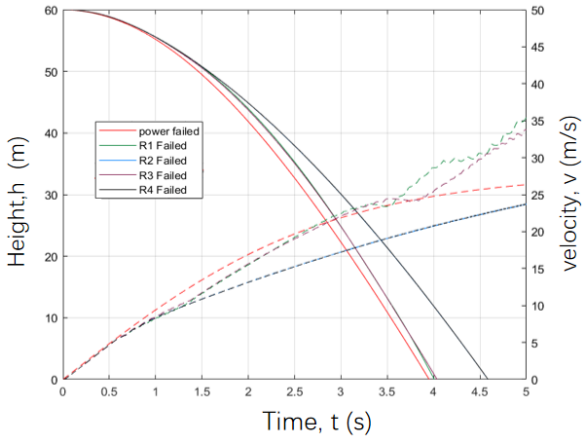


Fig. 8 Drone's velocity and altitude time history for initial forward velocity is 0 m/s with the flight control system.

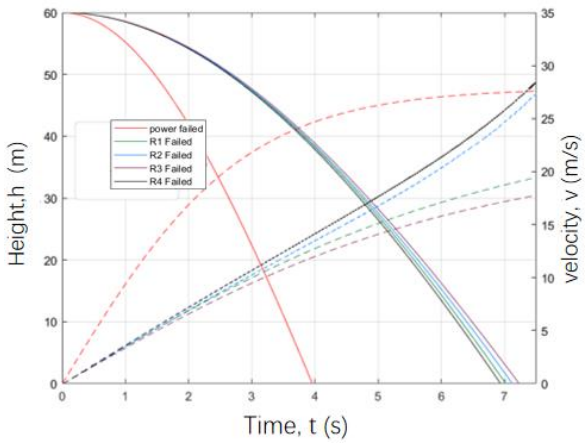


Fig. 9 Drone's velocity and altitude time history for initial forward velocity is 0 m/s without the flight control system.

**B. One (1) motor failed with/without flight control system (initial forward velocity: 8 m/s)**

When the initial forward velocity is 8 m/s and only one motor failed with working flight control system, the projection of the trajectory on the ground and the curve of UAV velocity and altitude time histories are shown in Fig. 11(a), Fig. 11(c), and Fig. 12, respectively. The possible collision area is small, distributed in a semi-circle with a radius less than 40 m which is around two times bigger compared to the initial velocity of 0 m/s.

When one motor (different position) with the control system failed at the same time, the possible collision area is larger along the velocity direction, and the trend of height and velocity changes with time is roughly bigger as when the initial velocity is 0 m/s with collision area distributed in a semi-circle with a radius of less than 90 m. the simulation results of the drone's trajectory, the projection of the trajectory on the ground, and the curve of UAV velocity and altitude with time are shown in Fig. 11(b), Fig. 11(d) and Fig. 13, respectively.

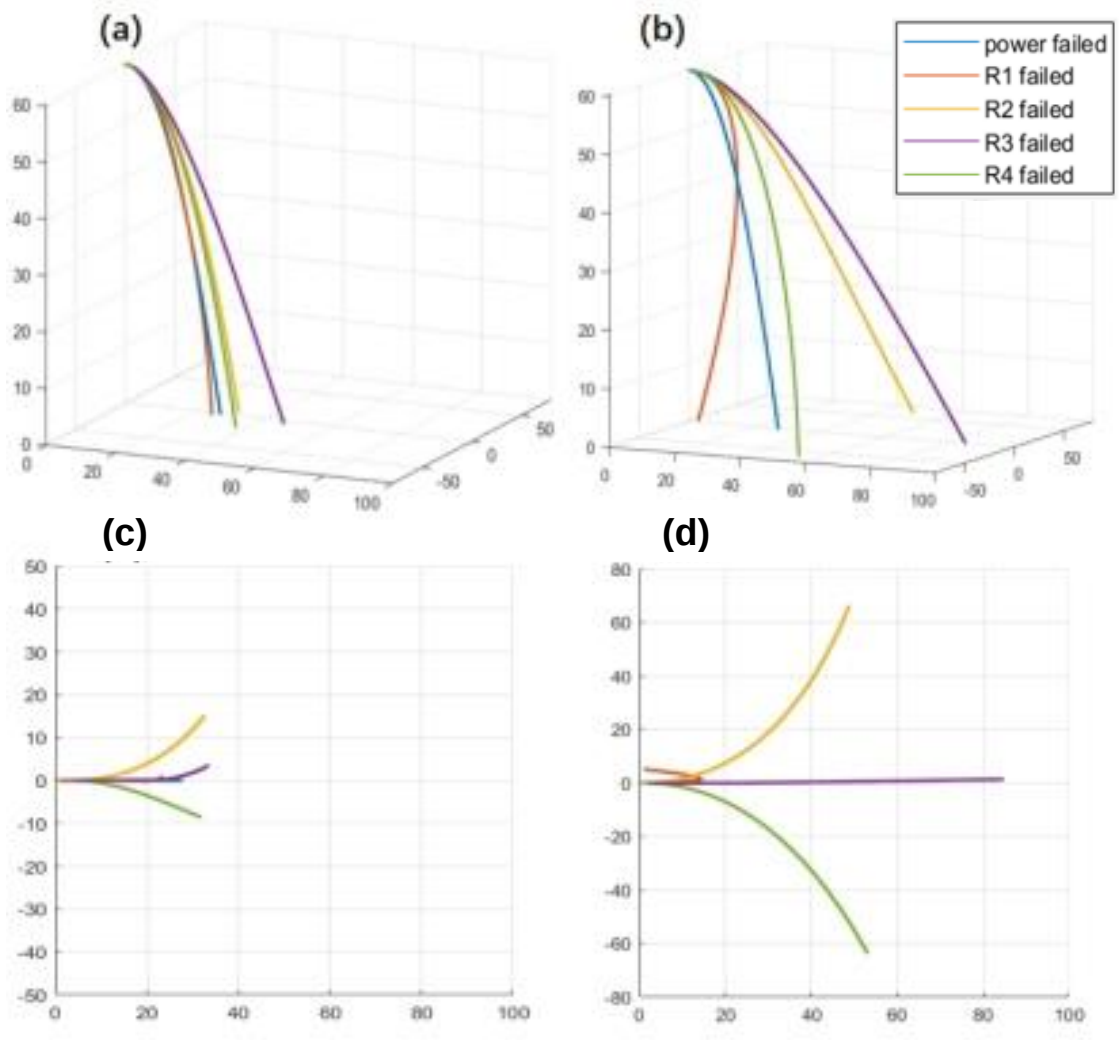


Fig. 10 Results for initial velocity is 8 m/s, one motor failed and with/without flight control system: (a) the trajectories when the flight control system is working; (b) the trajectories when flight control system failed; (c) projection of the trajectory on the ground when control system can work; and (d) projection of the trajectory on the ground when flight control system failed.

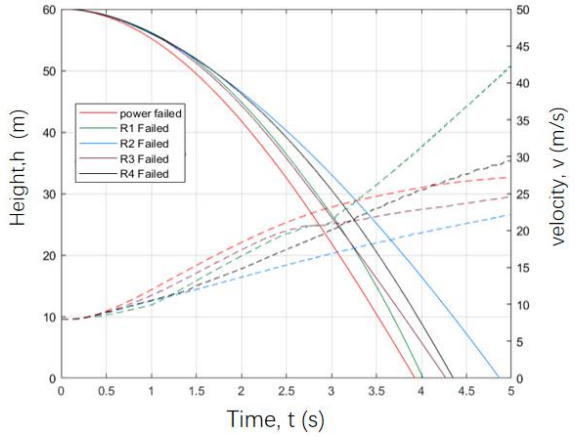


Fig. 11 Drone's velocity and altitude time history for initial velocity is 8 m/s with flight control systems.

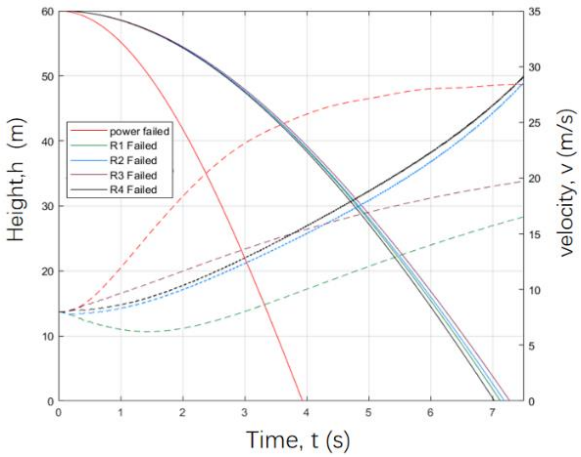


Fig. 12 Drone's velocity and altitude time history for initial velocity is 8 m/s without flight control systems.

**C. One (1) propeller of a motor fell-off**

When a blade of a specific motor is loose, no lift force is generated, but its torque still exists from the motor rotation. Hence the different initial velocities and assume that the control system can still work are defined in the simulation for this failure condition.

When the initial velocity is 0 m/s, the possible collision radius is 20 m, and in some cases, the impact velocity at the collision point is much faster than the case of power failure, reaching 45-50 m/s, the crash time is slightly shorter and the case of power failure. The simulation results of the drone's trajectory, the projection of the trajectory on the ground and the curve of UAV velocity and altitude with time are shown in Fig. 14(a), Fig. 14(c), and Fig. 15, respectively.

When the initial velocity is 8 m/s, the curve change trend in the simulation results is roughly the same as the corresponding single motor failure. The simulation results of the drone's trajectory, the projection of the trajectory on the ground and the curve of UAV velocity and altitude with time are shown in Fig. 14(b), Fig. 14(d), and Fig. 16, respectively.

**D. Two (2) different motors (R1-R4) failed**

For the situation when two different motors (R1-R4) failed, we consider the difference of initial velocity and assume that the control system can still work; this situation has the smallest possible collision area.

When the initial velocity is 0 m/s, the simulation results of the drone's trajectory, the projection of the trajectory on the ground and the curve of UAV velocity and height with time are shown in Fig. 17 (a), Fig. 17(c) and Fig. 18, respectively. When the initial velocity is 8 m/s, the simulation results of the drone's trajectory, the projection of the trajectory on the ground and the curve of UAV velocity and altitude with time are shown in Fig. 17(b), Fig. 17(d), and Fig. 19, respectively. When the initial velocity is 0 m/s, the possible collision radius at the height of 60 m is less than 5 m, but the collision velocity is higher than the case of dynamic failure, generally reaching 35 m/s and above, the collision time of motor failure at different positions is quite different.

When the original velocity is 8 m/s, if the drop point at the time of power failure is the center, the collision radius reaches 30 m, and in most cases, there is a greater collision velocity, but in rare cases, the trajectory will sway, and the velocity will start to slow down before impact.

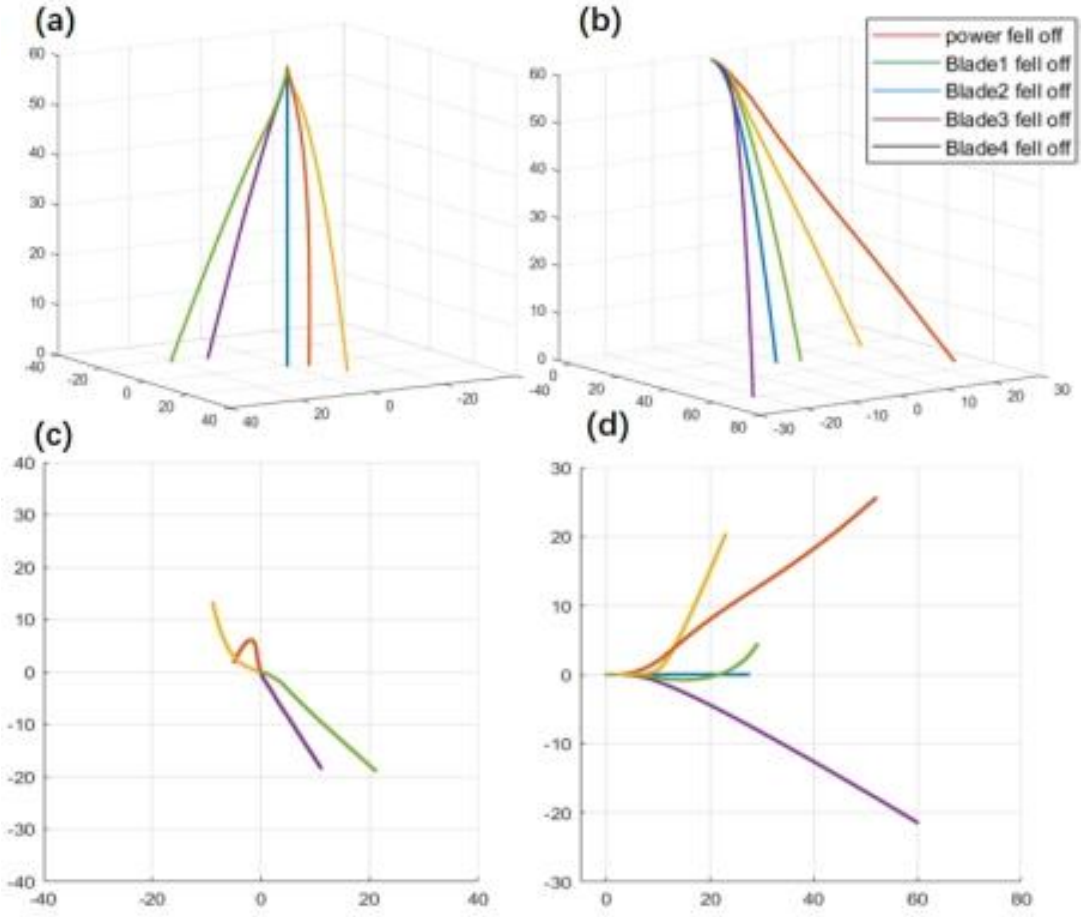


Fig. 13 Results for one blade fell off with flight control system is working: (a) the trajectories when initial velocity is 0 m/s; (b) the trajectories when initial velocity is 8 m/s; (c) projection of the trajectory on the ground when initial velocity is 0 m/s; and (d) projection of the trajectory on the ground when initial velocity is 8 m/s.

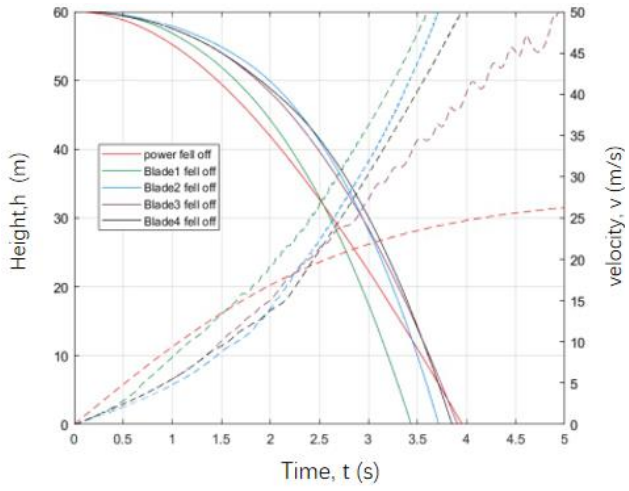


Fig. 14 Drone's velocity and altitude time history for initial forward velocity is 0 m/s, and one blade fell off.

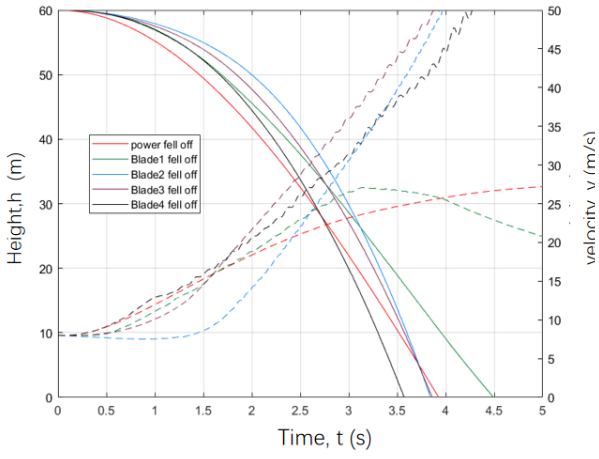


Fig. 15 Drone's velocity and altitude time history for initial forward velocity is 8 m/s, and one blade fell off.

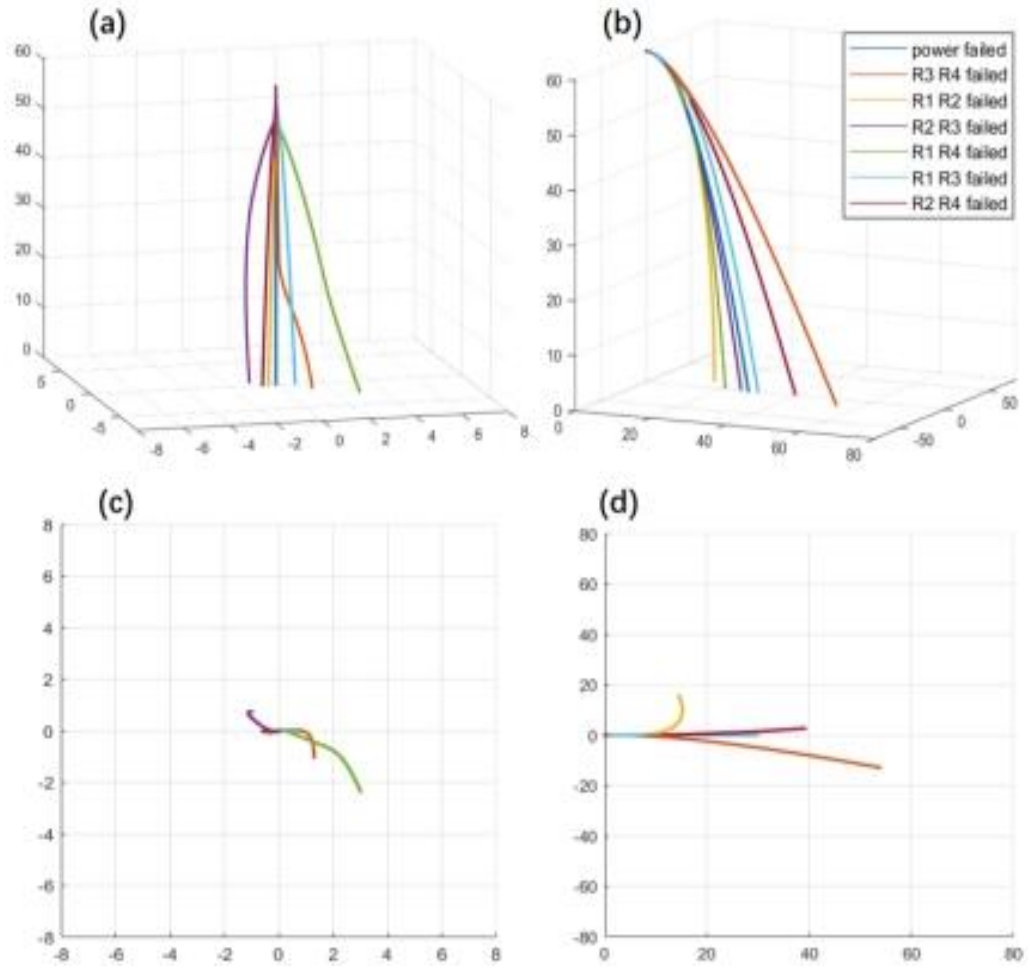


Fig. 16 Results for two motors failed with flight control system is working: (a) the trajectories when initial forward velocity is 0 m/s; (b) the trajectories when initial forward velocity is 8 m/s; (c) projection of the trajectory on the ground when initial forward velocity is 0 m/s; and (d) projection of the trajectory on the ground when initial forward velocity is 8 m/s.

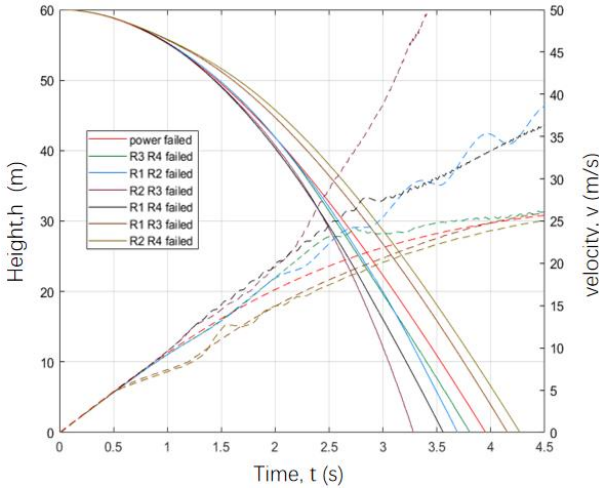


Fig. 17 Drone's velocity and altitude time history for initial velocity is 0 m/s, and two motors failed.

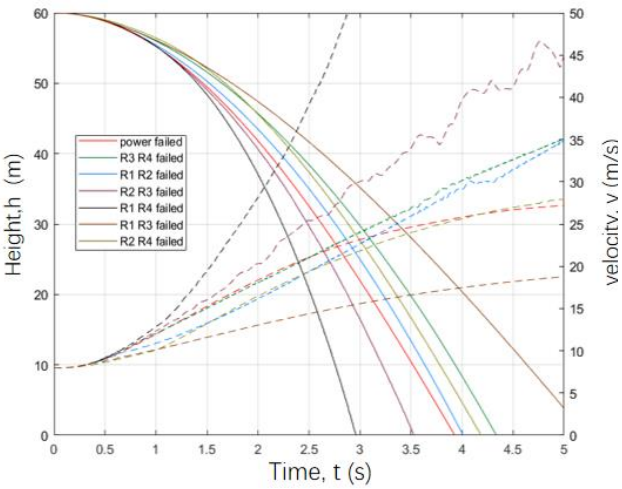


Fig. 18 Drone's velocity and altitude time history for initial forward velocity is 8 m/s, and two motors failed.

## VII. Concluding Remarks

The study investigates the effect of sUAV propulsion system failures that might lead to sUAV loss of thrust and crash to the ground. Four different sUAV failure modes, including single or multiple motor failures, control system failures, power failures, and blade loosening, have been considered.

Based on the possible failures of the quad-rotor UAV during the flight, this paper proposes a high-fidelity UAV mechanical model and uses a combination of ADAMS and MATLAB to perform a co-simulation to obtain the sUAV crash trajectory and the crash speed when the UAV propulsion system fails, the study concluded:

1. When a single motor fails, and the initial speed is 0 m/s (hovering), the possible crash area when the control system is still working is small, and the crash time is slightly longer compared to the case of power failure; moreover, the impact speed is not much different. When the control system fails, the crash time is noticeably longer than the case of power failure; in addition, the expected crash area is larger while the impact speed is lower than that of power failure in most cases. Similar simulation results can also be observed for the initial velocity of 8 m/s.
2. The case of single motor blade loosens and falls off, the crash time is not much different from the case of power failure, but the crash area is obviously larger than the case of a single motor failure, and this type of situation has the largest impact speed in various situations with has more complicated the crash trajectory
3. When the control system can continue to work, and two motors fail simultaneously, the possible crash area is slightly larger, and the possible impact speed is greater than the failure of a single motor. The results of motor failure at different positions are also quite different.

This study is preliminary works to identify the third-party risk to the ground (people, car, or building) due to sUAV crash caused by propulsion system failures for drone operation in the urban environment; validation works are important to verify the study done. Furthermore, the effect of other external factors that might influence UAV fault like a bird strike, mid-air collision with manned aviation [27], weather and communication signal deterioration can be considered in future works.

## Acknowledgements

This research is supported by the National Research Foundation, Singapore, and the Civil Aviation Authority of Singapore, under the Aviation Transformation Programme on Unmanned Aircraft Systems (UAS) in the topic of Third-Party Risks. The support from the Air Traffic Management Research institute (ATMRI) and the School of Mechanical and Aerospace Engineering (MAE), Nanyang Technological University (NTU) is also appreciated. Any opinions, findings, conclusions, or recommendations expressed in this material are those of the authors and do not reflect the views of National Research Foundation, Singapore, and the Civil Aviation Authority of Singapore.

## References

[1] Federal Aviation Administration (FAA), "FAA Aerospace Forecast FY2016-2036.,".

[2] Federal Aviation Administration (FAA), "Summary of small unmanned aircraft rule (Part 107) Federal Aviation Administration," 2016. Available: https://www.faa.gov/uas/media/part_107_summary.pdf.

[3] Civil Aviation Authority of Singapore (CAAS). "Air Navigation Act (Chapter 6). Air Navigation (101 — Unmanned Aircraft Operations) Regulations 2019.,", 2019.

[4] E. Petritoli, F. Leccese, and L. Ciani, "Reliability assessment of UAV systems," *IEEE International Workshop on Metrology for AeroSpace (MetroAeroSpace) June 2017*, p. 5, 2017, doi: 10.1109/MetroAeroSpace.2017.7999577.

[5] R. Melnyk, D. Schrage, V. Vitali, and H. Jimenez, "A third-party casualty risk model for unmanned aircraft system operations," *Reliability Engineering & System Safety*, vol. 124, p. 12, 2014, doi: https://doi.org/10.1016/j.ress.2013.11.016.

[6] S. H. Kim, "Third-Party Risk of Mid-Air Collision Between Small Unmanned Aircraft Systems," *AIAA Aviation Technology, Integration, and Operations Conference*, 2019, doi: https://doi.org/10.2514/6.2019-3052.

[7] Joint Authorities for Rulemaking of Unmanned Systems (JARUS), "JARUS guidelines on Specific Operations Risk Assessment (SORA),", 2019.

[8] K. D'Souza, T. Lyons, T. Lacy, and K. R. Kota, "Volume IV–UAS Airborne Collision Severity Evaluation–Engine Ingestion," 2017.

[9] M. H. Che Man, L. Hu, B. F. Ng, and K. H. Low, "Preliminary Evaluation of Thrust Loss in Commercial Aircraft Engine due to Airborne Collision with Unmanned Aerial Vehicles (UAVs)," p. 8, 2020, doi: 10.1109/ICUAS48674.2020.9214048.

[10] H. Liu, M. H. Che Man, and K. H. Low, "UAV airborne collision to manned aircraft engine: Damage of fan blades and resultant thrust loss," *Aerospace Science and Technology*, vol. 113, p. 106645, 2021/06/01/ 2021, doi: https://doi.org/10.1016/j.ast.2021.106645.

[11] X. Hu, B. Pang, F. Dai, and K. H. Low, "Risk Assessment Model for UAV Cost-Effective Path Planning in Urban Environments," *IEEE Access*, vol. 8, p. 12, 2020, doi: 10.1109/ACCESS.2020.3016118.
[12] C. E. Lin and P. C. Shao, "Failure Analysis for an Unmanned Aerial Vehicle Using Safe Path Planning," *Journal of Aerospace Information Systems*, vol. 17, no. 1, p. 12, 2017.
[13] J. Breunig, J. Forman, S. Sayed, L. Audenaerd, A. Branch, and M. Hadjimichael, "Modeling risk-based approach for small unmanned aircraft systems," p. 22, 2018, Art no. 18-1364. MITRE Corporation.
[14] A. l. Cour-Harbo, "Ground impact probability distribution for small unmanned aircraft in ballistic descent," *International Conference on Unmanned Aircraft Systems (ICUAS) September 2020*, p. 10, 2020, doi: 10.1109/ICUAS48674.2020.9213990.
[15] C. W. Lum and B. Waggoner, "A Risk Based Paradigm and Model for Unmanned Aerial Systems in the National Airspace," *Infotech@Aerospace March 2011*, Conference Paper 2012, doi: https://doi.org/10.2514/6.2011-1424.
[16] R. Aalmoes, Y. S. Cheung, E. Sunil, J. M. Hoekstra, and F. Bussink, "A conceptual third party risk model for personal and unmanned aerial vehicles," *International Conference on Unmanned Aircraft Systems (ICUAS) June 2015*, p. 9, 2015, doi: 10.1109/ICUAS.2015.7152424.
[17] J. V. Foster and D. C. Hartman, "High-Fidelity Multi-Rotor Unmanned Aircraft System (UAS) Simulation Development for Trajectory Prediction Under Off-Nominal Flight Dynamics," *AIAA Aviation Technology, Integration, and Operations Conference June 2017*, 2017, doi: https://doi.org/10.2514/6.2017-3271.
[18] E. Ancel, F. M. Capristan, J. V. Foster, and R. C. Condotta, "Real-time Risk Assessment Framework for Unmanned Aircraft System (UAS) Traffic Management (UTM)," *AIAA Aviation Technology, Integration, and Operations Conference June 2017*, p. 17, 2017, doi: https://doi.org/10.2514/6.2017-3273.
[19] A. I. Cour-Harbo, "Quantifying Risk of Ground Impact Fatalities for Small Unmanned Aircraft," *Journal of Intelligent & Robotic Systems*, vol. 93, p. 18, 2019, doi: https://doi.org/10.1007/s10846-018-0853-1.
[20] X. Zheng, He Yang, and J. Cheng, "Design and Implementation of UAV Flight Simulation Based on Matlab/Simulink," *Advances in Engineering Research*, 2015, doi: 10.2991/ameii-15.2015.34.
[21] R. A. Clothier and R. A. Walker, "The Safety Risk Management of Unmanned Aircraft Systems. Handbook of Unmanned Aerial Vehicles," 2014.
[22] OSD, "Unmanned Aerial Vehicle Reliability Study (Office of the Secretary of Defense, U.S. Department of Defense, 2003)," 2003.
[23] CAAS, "UA Safety Guidelines, Civil Aviation Authority Singapore (CAAS)," 2020. Available: https://www.caas.gov.sg/public-passengers/unmanned-aircraft/ua-safety-guidelines.
[24] H. Jintian and S. Huailin, "Quadrotor control simulation based on Adams and Matlab," *Automation and Information Engineering*, vol. 05, p. 4, 2012.
[25] T. Y. Chen, "Modeling and PID control for a quadrotor," 2018, doi: 10.19353/j.cnki.dzsj.2018.21.001.
[26] J. Lazatin, "A Method for Risk Estimation Analysis for Unmanned Aerial System Operation over Populated Areas," *AIAA Aviation Technology, Integration, and Operations Conference June* 2014, doi: 10.2514/6.2014-2284.
[27] M. H. Che Man and K. H. Low, "Damage Severity Prediction of Helicopter Windshields Caused by a Collision with a Small Unmanned Aerial Vehicle (sUAV)," AIAA Aviation Forum, 2021. Available: https://doi.org/10.2514/6.2021-3001.